Competitive Electron Transfer from the S_2 and S_1 Excited States of Zinc *meso*-Tetraphenylporphyrin to a Covalently Bound Pyromellitimide: Dependence on Donor−Acceptor Structure and Solvent

Ryan T. Hayes, Christopher J. Walsh, and Michael R. Wasielewski*

Department of Chemistry and Center for Nanofabrication and Molecular Self-Assembly, Northwestern University, Evanston, Illinois 60208-3113

Received: October 20, 2003; In Final Form: January 28, 2004

Zinc *meso*-tetraphenylporphyrin (ZnTPP) is known to have a relatively slow $S_2 \rightarrow S_1$ internal conversion rate, $(1-3\ ps)^{-1}$, so that electron transfer from S_2 to a nearby acceptor is possible. We have synthesized two zinc porphyrins in which a pyromellitimide (PI) acceptor is attached to the para position of a *meso*-phenyl group of the porphyrin (ZnTPP−PI) or to that of a β-phenyl group of the porphyrin (ZnTPP−β-PhPI). We report here on competitive electron transfer from the S_2 (excitation at 420 nm) and S_1 states (excitation at 550 nm) of these zinc porphyrins to PI in 2-methyltetrahydrofuran (MTHF) and toluene. Our transient absorption studies show that efficient electron transfer occurs from S_2 of ZnTPP to PI in these porphyrins despite the presence of the intervening phenyl between the zinc porphyrin macrocycle and the PI acceptor. Moreover, the results show that while charge separation from S_1 is about 6 times faster for PI attached to the *meso*-phenyl than for PI attached to the β-phenyl, the opposite is observed for charge separation from S_2. Subsequent charge recombination is 2.6−2.8 times faster for PI attached to the *meso*-phenyl relative to that of the β-phenyl. Comparisons of rates between MTHF and toluene show that the ordering of rates is the same for both solvents, although the rate ratios are larger in MTHF than in toluene.

Introduction

The relatively slow $S_2 \rightarrow S_1$ internal conversion rate, $(1-3\ ps)^{-1}$, of zinc *meso*-tetraphenylporphyrin (ZnTPP) has been the subject of several recent reports, which explore the dynamics of this process using mainly fluorescence upconversion techniques.[1−7] In some of these studies the ability of the S_2 state of zinc porphyrins to donate electrons to a covalently bound acceptor has also been investigated.[7−10] For example, LeGourrierec et al.[8] have investigated electron transfer from the S_2 state of ZnTPP to a covalently bound $Ru(bpy)_3$ (bpy = 2,2′-bipyridine) complex. In addition, Mataga and co-workers have studied the energy gap dependence for photoinduced electron-transfer rates from the S_2 state of the zinc porphyrin within a series of zinc 5-(aryleneimide (or arylenediimide))-10,20-diphenylporphyrins in which the nitrogen atom of the imide acceptor is directly bonded to the porphyrin macrocycle.[7,10] Given the limited lifetime of the zinc porphyrin S_2 state and the short donor−acceptor distances of most previously studied systems,[7,10] we wish to determine whether increasing the distance between the porphyrin macrocycle and a pyromellitimide (PI) electron acceptor within these molecules has a significant impact on the competition between electron transfer from the S_2 state of the zinc porphyrin and $S_2 \rightarrow S_1$ internal conversion. In addition, we wish to determine whether the rates of electron transfer from S_2 depend significantly on whether PI is attached to either the *meso* or β position of the zinc porphyrin. The two highest occupied molecular orbitals of zinc porphyrins have a_{1u} and a_{2u} symmetry. It is well-known that the a_{1u} orbital has significant electron density at the β carbons of the porphyrin with little density at the *meso* positions, while the opposite is true for the a_{2u} orbital.[11,12] Which of these two orbitals is the zinc porphyrin HOMO depends on the nature and the position of the substituents attached to the porphyrin. For example, when the *meso* positions (5,10,15,20) of the porphyrin are substituted with electron-donating groups, e.g. phenyl rings or alkyl chains, the a_{2u} orbital is the HOMO. On the other hand, substitution of the β positions with electron releasing groups, such as alkyl groups, results in the a_{1u} orbital being the HOMO. Generally, increased electron density at particular peripheral carbon atoms of the porphyrin results in stronger electronic coupling to molecules attached to those positions. If the attached molecule can accept energy and/or electrons from the porphyrin, the increased electronic coupling generally leads to increased rates of energy and/or electron transfer.[13,14] Ab initio configuration interaction calculations of porphyrin electronic states show that the configuration of the S_2 state has different contributions from the a_{1u} and a_{2u} orbitals than does that of the S_1 state.[15] For example, calculations on magnesium porphyrin show that its S_1 state has dominant contributions from its a_{2u} (HOMO) and a_{1u} (HOMO-1) orbitals, where the a_{2u} orbital has the larger coefficient (0.68) relative to that for the a_{1u} orbital (0.61). On the other hand, its S_2 state has a larger a_{1u} orbital coefficient (0.59) relative to that for the a_{2u} orbital (0.56). Thus attachment of the acceptor to the meso or β positions of the porphyrins may have an impact on electron-transfer rates from S_2. Last, we are interested in whether solvent properties affect the rates of electron transfer from S_2. Solvents can act to selectively stabilize or destabilize one or both of the a_{1u} or a_{2u} orbitals, thus changing the characteristics of the S_2 state itself.[16]

To examine these issues we have synthesized two zinc porphyrins, Chart 1, in which a PI acceptor is attached to the para position of a phenyl group at a *meso*-phenyl of the

* To whom correspondence should be addressed. E-mail: wasielew@chem.northwestern.edu.

10.1021/jp037176i CCC: $27.50
Published on Web 03/05/2004

CHART 1: Structures of Molecules Used in This Study

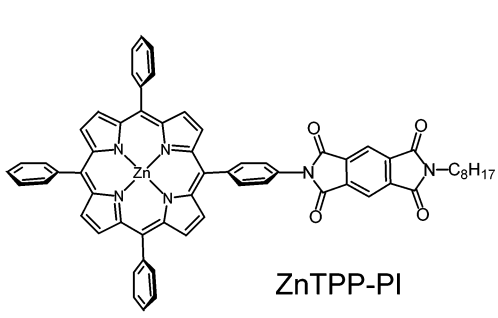

ZnTPP-PI

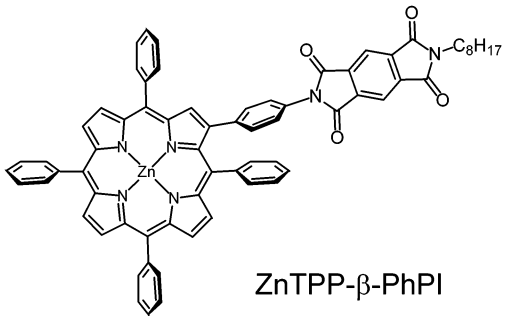

ZnTPP-β-PhPI

porphyrin (ZnTPP−PI) or to that of a β-phenyl group of the porphyrin (ZnTPP−β-PhPI). We report here on competitive electron transfer from the S_2 (excitation at 420 nm) and S_1 states (excitation at 550 nm) of ZnTPP−PI and ZnTPP−β-PhPI in 2-methyltetrahydrofuran (MTHF) and toluene. In this paper the S_1 and S_2 states of a given zinc porphyrin, ZnP, will be denoted as ^{1}*ZnP and ^{1}**ZnP, respectively.

Experimental Section

Synthesis. Proton nuclear magnetic resonance spectra were recorded on a Mercury 400 or Inova 500 NMR spectrometer using tetramethylsilane (TMS) as an internal standard. Laser desorption mass spectra were obtained with a PE Voyager DE-Pro MALDI-TOF mass spectrometer using 2-hydroxy-1-naphthoic acid or dithranol as a matrix. Solvents and reagents were used as received except for tetrahydrofuran (THF), which was purified on a basic alumina column. Flash and thin-layer chromatography was performed using Sorbent Technologies (Atlanta, GA) silica gel.

N-(n-Octyl)pyromellitic Monoanhydride (PIA). Benzene-1,2,4,5-dicarboxyanhyride (2.0 g, 9.2 mmol) is placed in 35 mL of dimethylformamide (DMF) and heated to 80 °C. *n*-Octylamine (1.2 g, 9.2 mmol) in 15 mL of DMF is added dropwise to the reaction flask over a period of 20 min. The reaction was heated at 80 °C for another 10 h to ensure completion. The reaction flask is removed from the heat, cooled to room temperature, and then placed in a freezer for 4 h. Disubstituted PI precipitates and is removed by filtration and centrifugation. The DMF filtrate is then evaporated and the tacky residue is redissolved in dichloromethane (DCM). Some unreacted starting material precipitates from DCM as a white solid and is easily filtered off. The filtrate is evaporated to the minimal amount of DCM necessary to maintain solubility, and then the product is precipitated by pouring the reaction mixture into a large volume of hexane. The precipitate is recovered through centrifugation. Further purification is achieved by flash silica chromatography using a solvent gradient starting with 95/5 DCM/ethyl acetate (v/v) and going to 80/20 DCM/ethyl acetate. Unreacted starting material precipitates out on top of the silica column and does not elute as long as the eluent is mainly DCM. After the column, the tacky material is recrystallized from hot acetic anhydride to yield PIA (2.0 g, 33%). ^{1}H NMR ($CDCl_3$): δ 8.43 (d, J = 0.64 Hz, benzene, 2H); 3.76 (t, J = 7.37 Hz, *n*-methylene, 2H); 1.71 (quint., J = 7.13 Hz, methylene, 2H); 1.32 (m, methylene, 11H); 0.86 (t, J = 6.76 Hz, methyl, 3H). MALDI-MS: 328.9 (329.4, calcd).

N-(4-Bromophenyl)-N′-(n-octyl)pyromellitimide. 4-Bromoaniline (0.522 g, 3.0 mmol) and PIA (1.0 g, 3.0 mmol) were reacted in DMF at 120 °C for 4 h. Upon cooling to room temperature, the product precipitated. The creamy-white solid was filtered and dried to yield *N*-(4-bromophenyl)-*N′*-(*n*-octyl)-pyromellitimide (1.0 g, 2.1 mmol, 68%). ^{1}H NMR ($CDCl_3$): δ 8.37 (s, pyromellitimide, 2H); 7.66 (d, J = 8.72 Hz, phenyl, 2H); 7.37 (d, J = 8.68 Hz, phenyl, 2H); 3.75 (t, J = 7.36 Hz, *n*-methylene, 2H); 1.70 (t, J = 6.88 Hz, methylene, 2H); 1.31 (m, methylenes, 10H); 0.86 (m, methyl, 3H). MALDI-MS: 483.1 (483.4, calcd).

N-[4-(Tributyltin)phenyl)]-N′-(n-octyl)pyromellitimide. Reaction of (4-bromophenyl)pyromellitimide (1.6 g, 3.3 mmol) with bis-tributyltin (5.77 g, 9.9 mmol) in dry refluxing toluene for 14 h under a nitrogen atmosphere using tetrakis(triphenylphosphine)palladium(0) as the catalyst gave *N*-[4-(tributyltin)-phenyl)]-*N′*-(*n*-octyl)pyromellitimide, which was isolated using column chromatography (2.4 g, 67%). ^{1}H NMR ($CDCl_3$): δ 8.38 (s, pyromellitimide, 2H); 7.63 (d, J = 8.21 Hz, phenyl, 2H); 7.39 (d, J = 8.22 Hz, phenyl, 2H); 3.76 (t, J = 7.36 Hz, *n*-methylene, 2H); 1.72 (t, J = 6.89 Hz, methylene, 2H); 1.55 (m, methylene, 6H); 1.34 (m, methylene, 16H); 1.09 (m, methylene, 6H); 0.89 (m, methyl, 12H).

ZnTPP−PI. (5-Bromo-10,15,20-triphenylporphyrinato)zinc-(II)[17,18] was prepared from 5,10,15-triphenylporphyrin.[19] Pd_2dba_3 (5 mg, dba = dibenzylideneacetone) and P(*o*-tolyl)$_3$ (50 mg) were dissolved in 2 mL DMF. To the reaction mixture was added 5-bromo-10,15,20-triphenylporphyrinatozinc(II) (32 mg, 0.047 mmol), and the flask was immersed in an oil bath at 70 °C. In a separate flask, *N*-[4-(tributyltin)phenyl)]-*N′*-(*n*-octyl)-pyromellitimide (32 mg, 0.047 mmol) was dissolved in 2 mL of DMF. The tin derivative was added to the reaction mix, and 10 mol % of CuI was added. The reaction was stirred overnight under nitrogen. After 24 h, the reaction was cooled, DMF removed under vacuum, and the residue deposited onto silica gel. Column chromatography in 75/25 (v/v) chloroform/hexanes gave pure ZnTPP−PI (25 mg, 52%). ^{1}H NMR ($CDCl_3$): δ 9.01 (m, porph, 8H); 8.39 (d, J = 8.50 Hz, bridge phenyl, 2H); 8.34 (s, pyromellitimide, 2H); 8.24 (m, *o*-phenyl, 6H); 7.86 (d, J = 8.72 Hz, bridge phenyl, 2H); 7.78 (m, *m*,*p*-phenyl, 9H); 3.72 (t, J = 7.36 Hz, *n*-methylene, 3H); 1.71 (m, methylene, 2H); 1.31 (m, methylene, 10H); 0.89 (m, methyl, 3H). MALDI-MS: 1004.2 (1004.5, calcd).

ZnTPP−β-PhPI. Pd_2dba_3 (5 mg) and P(*o*-tolyl)$_3$ (50 mg) were dissolved in 2 mL of DMF. To the reaction mix was added (2-bromo-5,10,15,20-tetraphenylporphyrinato)zinc(II)[20] (0.150 g, 0.198 mmol), and the flask was immersed in an oil bath at 70 °C. In a separate flask, *N*-[4-(tributyltin)phenyl)]-*N′*-(*n*-octyl)-pyromellitimide (0.206, 0.297 mmol) was dissolved in 2 mL of DMF. The tin derivative was added to the reaction mix, and 10 mol % of CuI was added. The reaction was stirred overnight under nitrogen. After 24 h, the reaction was cooled, the DMF was removed under vacuum, and the residue was deposited onto silica gel. Column chromatography using 75/25 (v/v) chloroform/hexanes gave pure ZnTPP−β-PhPI (133 mg, 62%). ^{1}H NMR ($CDCl_3$): δ 8.91 (m, porph, 7H); 8.41 (s, pyromellitimide, 2H);

TABLE 1: Absorption Maxima for the Zinc Porphyrin Soret and *Q*(0,0) Bands in MTHF and Toluene and Energies for S_1, S_2, and the Radical Ion Pairs

	Soret (nm)		*Q*(0,0) (nm)		E_{S1} (eV)		E_{S2} (eV)		ΔG_{IP} (eV)	
compound	MTHF	toluene.	MTHF	toluene	MTHF	toluene	MTHF	toluene	MTHF	toluene
ZnTPP	423	424	595	589	2.08	2.09	2.92	2.90		
ZnTPP−PI	423	424	595	589	2.07	2.09	2.91	2.90	1.63	2.06
ZnTPP−β-PhPI	426	427	598	591	2.06	2.07	2.88	2.88	1.63	2.04

8.21 (m, *o*-phenyl, 6H); 7.90 (d, $J = 7.51$ Hz, *o*-phenyl, 2H); 7.76 (m, *m*,*p*-phenyl, 9H); 7.49 (d, $J = 8.45$ Hz, bridge-phenyl, 2H); 7.38 (t, $J = 7.49$ Hz, *m*-phenyl, 2H); 7.30 (t, $J = 7.14$ Hz, *p*-phenyl, 1H); 7.21 (d, $J = 8.34$ Hz, bridge-phenyl, 2H); 3.77 (t, $J = 7.26$ Hz, *N*-methylene, 2H); 1.75 (quintet, $J = 7.15$ Hz, methylene, 2H); 1.31 (m, methylene, 10H); 0.92 (m, methyl, 3H). MALDI-MS: 1079.9 (1080.6, calcd).

Spectroscopy. Femtosecond transient absorption measurements were made using a regeneratively amplified titanium sapphire laser system operating at a 2 kHz repetition rate outfitted with a CCD array detector (Ocean Optics PC2000) for simultaneous collection of spectral and kinetic data.[21] The frequency-doubled output from the laser was used to provide 420 nm, 130 fs pulses for excitation, while 550 nm, 130 fs excitation pulses were produced using an optical parametric amplifier.[22] A white light continuum probe pulse was generated by focusing the 840 nm fundamental into a 1 mm sapphire disk. All-reflective optics were used to focus the 840 nm pulse into the sapphire and recollimate the white light output, thus limiting the chirp on the white light pulse to less than 200 fs from 450 to 800 nm. Cuvettes with a 2 mm path length were used, and the samples were irradiated with 0.5 μJ/pulse focused to a 200 μm spot. The optical density at the excitation wavelength was typically 0.3−0.5. The samples were stirred during the experiment using a wire stirrer to prevent thermal lensing and sample degradation. The total instrument response for the pump−probe experiments was 180 fs. Steady-state absorption and emission spectra were performed on a Shimadzu 1601 UV/vis spectrophotometer and PTI instruments single-photon-counting spectrofluorimeter, respectively. A 10 mm quartz cuvette was used with optical density at 425 nm maintained at 0.1 ± 0.05 to avoid reabsorption artifacts. All solvents were spectrophotometric grade. Toluene was purified by passing it through series CuO and alumina columns (GlassContour), while 2-methyltetrahydrofuran (MTHF; Aldrich) was purified by passing it through a basic alumina column immediately prior to use.

Kinetic analyses were performed at several wavelengths using a nonlinear least-squares fit to either a general sum-of-exponentials function or to a series A → B → C kinetic mechanism using the Levenberg−Marquardt method[23] accounting for the presence of the finite instrument response. The wavelength for these analyses centers on the relatively narrow PI^- band at 720 nm.[24] Kinetic simulations were carried out using the CKS program developed by the IBM Almaden Research Center.

Electrochemical measurements were performed using a CH Instruments Model 622 electrochemical workstation. The solvent was butyronitrile (PrCN) containing 0.1 M tetra-*n*-butylammonium perchlorate electrolyte. A 1.0 mm diameter platinum disk electrode, a platinum wire counter electrode, and a Ag/Ag_xO reference electrode were employed. The ferrocene/ferrocinium couple (Fc/Fc^+, 0.52 vs SCE) was used as an internal reference for all measurements. The energies of the radical ion pairs given in Table 1 were calculated[25] using the one-electron oxidation potentials of the zinc porphyrins (0.85 V vs SCE), the one-electron reduction potential of PI (−0.71 vs SCE), ionic radii of 7 Å and 5 Å, respectively, for the zinc porphyrins and PI, and donor−acceptor distances of 13.1 Å (ZnTPP−PI) and 13.5 Å (ZnTPP−β-PhPI). The total reorganization energies for the electron-transfer reactions $\lambda_{CS} = \lambda_{CR} = 0.33$ eV in toluene and 0.86 eV in MTHF were calculated using the dielectric continuum expression of Marcus.[26]

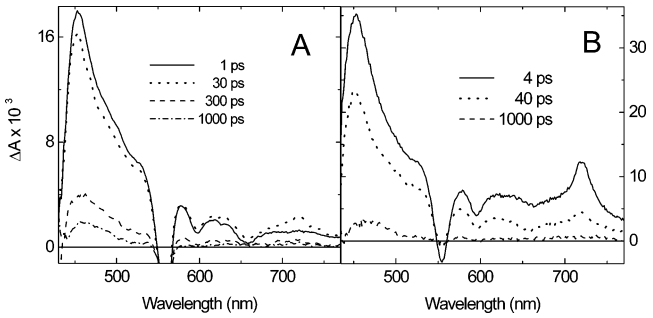

Figure 1. Transient absorption spectra for ZnTPP−PI in MTHF with (A) 550 and (B) 420 nm excitation.

Results

The advantages of employing PI as an electron acceptor have been well-documented.[24,27−34] The sharp transient absorption feature of PI^- near 720 nm ($\epsilon = 41\,700$ M^{-1} cm^{-1})[24] allows for kinetic analyses of the electron-transfer reactions with minimal interference from the zinc porphyrin features. It is well-known that strong, overlapping optical absorptions of ^{1}*ZnTPP and $ZnTPP^+$ occur mainly at 460−470 nm and that $ZnTPP^+$ has a broad absorption feature around 650 nm as well, which is more pronounced when the zinc porphyrin is an octaalkylporphyrin.[12,28,32] While PI^- also has a second, lower intensity absorption at 652 nm ($\epsilon = 9800$ M^{-1} cm^{-1}), we will not rely on this feature because it overlaps with the absorption of both $ZnTPP^+$ and ^{1}*ZnTPP. The onset of ^{1}*ZnTPP fluorescence at 650 nm, which appears as a stimulated emission feature (an absorbance bleach) in the transient absorption experiments, can also be used to monitor the lifetime of S_2.

The optical absorption maxima of the Soret and *Q*(0,0) bands for each compound and ZnTPP in MTHF and toluene are listed in Table 1. The Soret band maxima are nearly solvent-independent, while the *Q*(0,0) band maxima show consistent, small red shifts of their absorption maxima in MTHF relative to toluene. These shifts are most likely due to ligation of the MTHF oxygen atom to the zinc atom in each case. The S_1 and S_2 energy levels of each molecule were determined by averaging the energies of the *Q*(0,0) and Soret band absorptions of the zinc porphyrin with those of the corresponding emission maxima.

Excitation of ZnTPP−PI in MTHF at 550 nm produces the transient absorption spectra shown in Figure 1A. The spectrum at 1 ps shows the presence of ^{1}*ZnTPP alone, while by 30 ps $ZnTPP^+-PI^-$ has formed, as evidenced by the small peak at 720 nm. The PI^- band appears with $\tau = 17$ ps and is assigned to the formation of $ZnTPP^+-PI^-$, which subsequently decays with $\tau = 140$ ps. The weak 480 nm feature at 1000 ps seen in Figure 1A is due to ^{3}*ZnTPP formed by radical pair intersystem crossing, which, although not unprecedented,[35] is somewhat

TABLE 2: Summary of Transient Absorption Kinetic Data[a]

compound	solvent	λ_{EXC} (nm)	λ_{PR} (nm)	τ_{R1} (ps)	A_{R1} (%)	τ_{R2} (ps)	A_{R2} (%)	τ_{D1} (ps)	A_{D1} (%)	τ_{D2} (ps)	A_{D2} (%)
ZnTPP−PI	MTHF	550	720	17	100			140	100		
ZnTPP−PI	MTHF	420	720	1.4	100			18	80	150	20
ZnTPP−PI	MTHF	550	480	0.3	90	18	10	0.3	15	140	85
ZnTPP−PI	MTHF	420	480	0.5	80	18	20	0.6	15	160	85
ZnTPP−β-PhPI	MTHF	550	720	96	100			370	85	>6 ns	15
ZnTPP−β-PhPI	MTHF	420	720	0.7	50	9.7	50	380	95	>6 ns	5
ZnTPP−PI	toluene	550	720	120	100			700	100		
ZnTPP−PI	toluene	420	720	0.6	57	127	43	610	100		
ZnTPP−β-PhPI	toluene	550	720	0.2	100			>6 ns	100		
ZnTPP−β-PhPI	toluene	420	720	0.4	100			2.0 ns	100		

[a] τ_{R1}, τ_{R2}, A_{R1}, and A_{R2} are the time constants and their respective amplitudes for the rise of the PI^- absorption, while τ_{D1}, τ_{D2}, A_{D1}, and A_{D2} are the time constants and their respective amplitudes for the decay of the PI^- absorption. The 0.2 ps instrument response function has been deconvoluted from the data. The S_2 lifetimes of ZnTPP in MTHF and toluene are 2.3 and 1.1 ps, respectively.

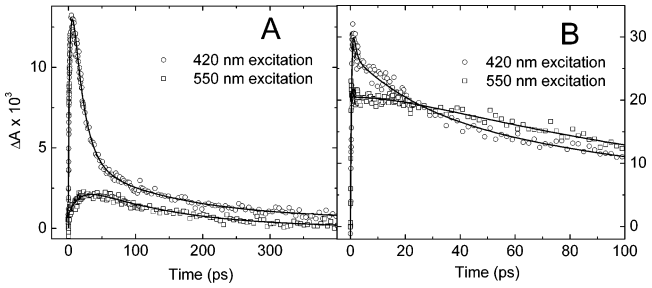

Figure 2. Transient absorption kinetics of ZnP−PhPI in MTHF probed at (A) 720 and (B) 480 nm. Solid lines are exponential fits.

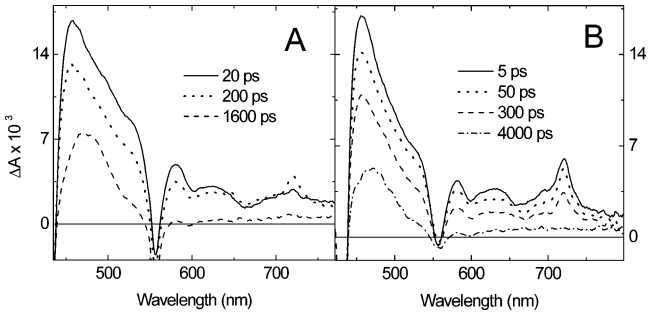

Figure 3. Transient absorption spectra of ZnTPP−β-PhPI in MTHF with (A) 550 and (B) 420 nm excitation.

unusual given that this process is generally inefficient for short-lived radical ion pairs.[36] The corresponding spectra for 420 nm excitation are given in Figure 1B. The spectrum at 2 ps already reveals an intense PI^- feature at 720 nm. The transient absorption kinetic traces at 720 nm shown in Figure 2A reveals that this absorption appears with $\tau = 1.4$ ps and decays biexponentially with $\tau = 18$ and 140 ps. Moreover, the transient absorption kinetics at 480 nm requires 18 ps rise and 140 ps decay components to fit the data, Figure 2B. The kinetic components and their amplitudes are listed in Table 2. For completeness, transient absorption spectra of ZnTPP in MTHF at 0.4 ps ($S_2 \rightarrow S_n$) and 20 ps ($S_1 \rightarrow S_n$) following 420 nm excitation are given in the Supporting Information, Figure S1.

The transient absorption spectra for ZnTPP−β-PhPI in MTHF following 550 nm excitation are shown in Figure 3A. At 20 ps the transient spectrum is due to ^{1}*ZnTPP (see Figure S1), while by 200 ps a feature due to PI^- has appeared at 720 nm. After 1600 ps, the only species remaining is ^{3}*ZnTPP. Transient absorption kinetics obtained at 720 nm, Figure 4A and Table 2, show that the charge separation reaction: ^{1}*ZnTPP−β-PhPI $\rightarrow$ $ZnTPP^+$−β-$PhPI^-$ is about six times slower than the corresponding reaction for ZnTPP−PI. Once again, the formation of ^{3}*ZnTPP is evident at long times. The spectrum following 420 nm excitation shows a significant PI^- peak at 5 ps, Figure 3B, which occurs substantially earlier than is observed following 550 nm excitation. Figure 4A shows kinetic traces for both excitation wavelengths. Electron transfer from S_2 is competitive with internal conversion, and the kinetic traces show that PI^- is formed rapidly ($\tau = 0.7$ ps) relative to that produced from S_1 ($\tau = 96$ ps). At 650 nm, Figure 4B, the exponential fit of the initial, fast decay process reveals that the stimulated emission onset occurs with $\tau = 0.7$ ps in agreement with the faster of the two time constants for the formation of PI^-. Note that the stimulated emission onset is the decaying transient feature in the kinetic trace, i.e., the appearance of the bleach due to stimulated emission. The initial rise of the signal is due to the formation of the $S_2 \rightarrow S_n$ absorption convolved with the 0.2 ps instrument response function.

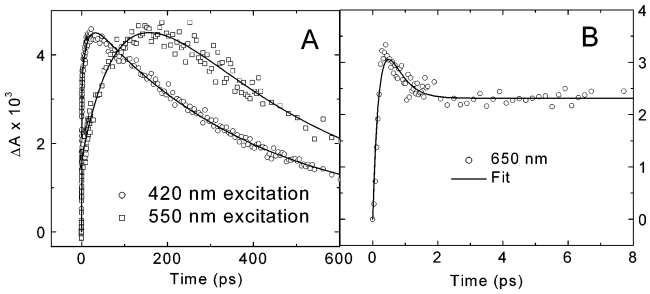

Figure 4. Transient absorption kinetics of ZnTPP−β-PhPI in MTHF (A) at 720 nm using 420 and 550 nm excitation and (B) at 650 nm using 420 nm excitation. Solid lines are exponential fits.

The slower $\tau = 9.7$ ps component for the PI^- formation observed at 720 nm may be due to spectral narrowing resulting from vibrational relaxation. Interestingly, kinetic components readily assignable to vibrational and/or solvent relaxation are not observed for ZnTPP−PI in either solvent or for ZnTPP−β-PhPI in toluene. While it is possible that these relaxation processes are very fast in these cases, it is more likely that the kinetic components due to vibrational and solvent relaxation occur with similar time constants as do charge separation and recombination, so that the relative contributions of the various processes cannot be easily separated. This is evident from the kinetic components given in Table 2. For example, the electron-transfer rates from S_1 for both ZnTPP−PI and ZnTPP−β-PhPI in either solvent are all slow, making it difficult to discern an additional component on the 10 ps time scale, especially if it has a low amplitude.

Excitation of ZnTPP−PI in toluene with 550 nm pulses produces transient absorption spectra similar to those shown for ZnTPP−PI in MTHF, Figure 5A. The transient spectrum at 10 ps is dominated by ^{1}*ZnTPP and evolves by 150 ps into the spectrum of $ZnTPP^+$−PI^-, which decays more slowly to give an intense spectrum due to ^{3}*ZnTPP by 4.5 ns. The correspond-

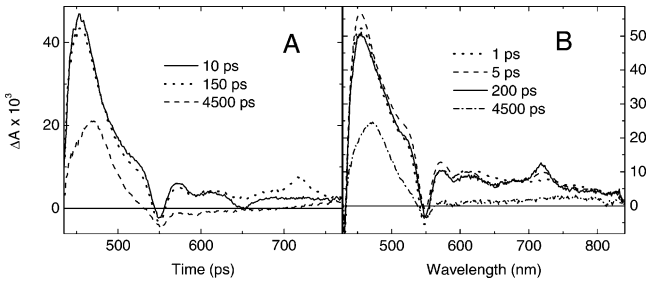

Figure 5. Transient absorption spectra of ZnTPP−PI in toluene with (A) 550 and (B) 420 nm excitation.

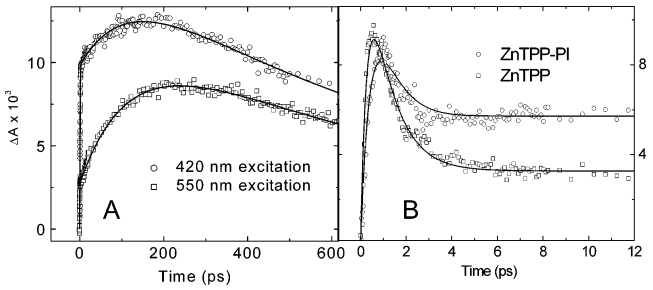

Figure 6. Transient absorption kinetics of ZnTPP−PI in toluene (A) at 720 nm with 420 and 550 nm excitation and (B) at 650 nm with 420 nm excitation. Solid lines are exponential fits.

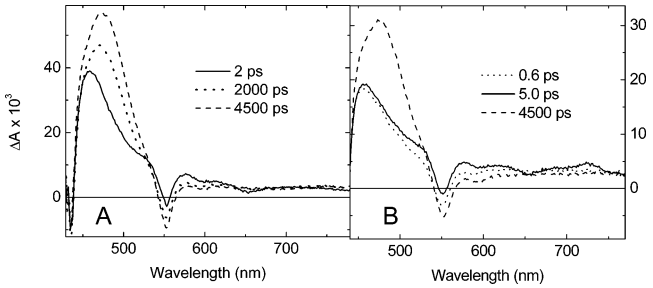

Figure 7. Transient absorption spectra of ZnTPP−β-PhPI in toluene with (A) 550 and (B) 420 nm excitation.

ing data for ZnTPP−PI excited at 420 nm results in formation of ZnTPP$^+$−PI$^-$ from the S_2 state of ZnTPP as evidenced by the appearance of the PI$^-$ band in the transient absorption spectrum at 5 ps, Figure 5B. A comparison between the transient kinetics for PI$^-$ formation monitored at 720 nm is shown in Figure 6A. It is evident from the data in Figure 6A that 420 nm excitation results in a significant increase in radical ion pair production at early times relative to that produced by 550 nm excitation. Figure 6B compares the kinetics of the onset of stimulated emission for ZnTPP and ZnTPP−PI in toluene monitored at 650 nm. The onset for ZnTPP occurs with $\tau =$ 1.1 ps, while that for ZnTPP−PI occurs with $\tau = 0.6$ ps. The latter value matches the fast component for PI$^-$ formation following 420 nm excitation of ZnTPP−PI.

Excitation of ZnTPP−β-PhPI in toluene with 550 nm laser pulses produces transient absorption spectra that show no indication of ion pair formation, Figure 7A, while excitation with 420 nm pulses shows the presence of PI$^-$ at 5 ps. Direct formation of ^{1}*ZnTPP using 550 nm excitation is followed by spin−orbit-induced intersystem crossing to yield ^{3}*ZnTPP over the 6 ns time course of the experiment as indicated by the strong 480 nm feature[37] in the spectrum at 4.5 ns. Figure 7B shows that ZnTPP$^+$−β-PhPI$^-$ undergoes radical ion pair intersystem crossing followed by charge recombination to ultimately yield ^{3}*ZnTPP as well. The transient absorption kinetics for the formation of PI$^-$ at 720 nm, Figure 8A, and the onset of stimulated emission due to formation of S_1 at 650 nm, Figure

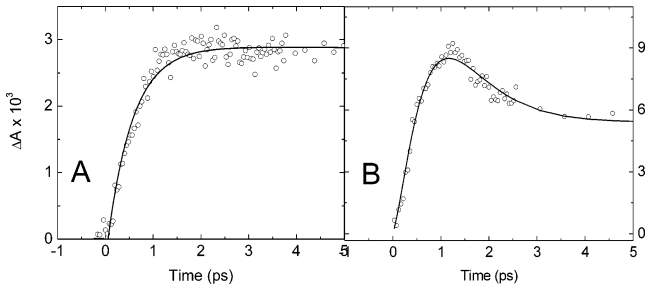

Figure 8. Transient absorption kinetics for ZnTPP−β-PhPI in toluene using 420 nm excitation and probed at (A) 720 and (B) 650 nm. The solid lines are exponential fits.

TABLE 3: Electron-Transfer Rate Constants

compound	solvent	k_{CS1} (s^{-1})	k_{CS2} (s^{-1})	ϕ_{CS2} (%)	k_{CR} (s^{-1})
ZnTPP−PI	MTHF	5.8×10^{10}	2.8×10^{11}	39	7.1×10^{9}
ZnTPP−β-PhPI	MTHF	1.0×10^{10}	9.9×10^{11}	69	2.7×10^{9}
ZnTPP−PI	toluene	8.3×10^{9}	7.6×10^{11}	46	1.4×10^{9}
ZnTPP−β-PhPI	toluene		1.6×10^{12}	64	5.0×10^{8}

8B, both show that charge separation from ^{1}**ZnTPP occurs very rapidly with $\tau = 0.4$ ps (following deconvolution of the 0.2 ps instrument response function).

Discussion

The rate constants for electron transfer from ^{1}*ZnTPP to PI, k_{CS1}, given in Table 3 are obtained using the following expression: $k_{CS1} = (1/\tau_{obs}) - (1/\tau_{S1})$, where τ_{obs} is the observed time constant for the formation of the radical ion pair and τ_{S1} is the lifetime of ^{1}*ZnTPP, which is 2.4 ns. To obtain the corresponding rate constants for electron transfer from ^{1}**ZnTPP to PI, we assume that S_2 is initially and selectively populated by one-photon absorption at 420 nm. The observed time constant, k_{obs}, for the decay of the stimulated emission band at 650 nm and the appearance of the PI$^-$ band at 720 nm is $k_{obs} = k_{CS2} + k_{IC}$, where k_{CS2} is the rate constant for charge separation from S_2 and k_{IC} is the rate constant for $S_2 \rightarrow S_1$ internal conversion. This expression assumes that vibrational relaxation and solvent dynamics can be distinguished from the initial charge separation event. In general, however, as has been discussed above, this assumption is not always valid. The values of k_{IC} for ZnTPP in toluene and MTHF are $(1.1\ ps)^{-1}$ and $(2.3\ ps)^{-1}$, respectively, as determined from the onset of stimulated emission at 650 nm following 420 nm excitation. Fluorescence upconversion studies have shown that the $S_2 \rightarrow S_1$ internal conversion rates for ZnTPP in benzene and THF are similar to those we obtain in toluene and MTHF.[7,38]

Figure 9 shows that the radical ion pair energy levels for ZnTPP−PI and ZnTPP−β-PhPI are nearly isoenergetic with that of ^{3}*ZnTPP in MTHF, while they are nearly isoenergetic with that of ^{1}*ZnTPP in toluene. The observed rate constants for charge separation from S_1 of both ZnTPP−PI and ZnTPP−β-PhPI, Table 3, increase as the solvent polarity increases and the energy levels of the radical ion pairs are stabilized in MTHF relative to toluene. For example, the charge separation rate for ZnTPP−PI in MTHF is about 7 times faster than in toluene. The free energies for charge separation from S_1 in MTHF and toluene are about −0.45 and −0.05 eV, respectively, while the corresponding values of the total reorganization energies are 0.86 and 0.33 eV, so that the observed increase in rate as the free energy of reaction becomes more negative is consistent with both charge separation reactions being in the normal region of the Marcus rate vs free energy profile.[26,39] A similar comparison for ZnTPP−β-PhPI cannot be made because the

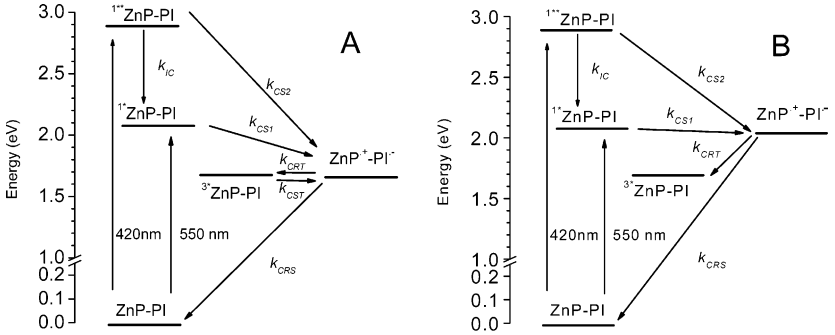

Figure 9. Energy level diagrams for ZnP−PI systems in (A) MTHF and (B) toluene. The energy levels for all four compounds are within ±0.05 V of the energies indicated.

charge separation rate from S_1 in toluene is too slow to compete with the decay of S_1. On the other hand, making the same comparisons for charge separation from S_2 in ZnTPP−PI and ZnTPP−β-PhPI shows that the rates of charge separation are 2−3 times faster in toluene for each molecule relative to MTHF, just the opposite from that observed for charge separation from S_1. The free energies of reaction for charge separation from S_2 for both ZnTPP−PI and ZnTPP−β-PhPI in MTHF and toluene are about −1.3 and −0.8 eV, respectively, while the corresponding values of the total reorganization energies are 0.86 and 0.33 eV, so that the rate data are consistent with both charge separation reactions from S_2 being in the Marcus inverted region.

A consequence of the fact that the energy of $ZnTPP^+-PI^-$ is nearly isoenergetic with that of ^{3}*ZnTPP in MTHF is the observed biexponential nature of the decay of $ZnTPP^+-PI^-$, Figure 2A. The kinetic data suggest that there is a rapid equilibrium between $ZnTPP^+-PI^-$ and the nearly isoenergetic ^{3}*ZnTPP state. Simulation of the kinetic data using the mechanism outlined in Figure 9A reveals that the dominant short component results from rapid radical ion pair recombination to ^{3}*ZnTPP with $k_{CRT} = 5.9 \times 10^{10}$ s^{-1}, while the longer component is due to repopulation of the radical ion pair state with $k_{CST} = 3.3 \times 10^{10}$ s^{-1} followed by recombination of the radical pair leading to ground state with $k_{CRS} = 7.0 \times 10^9$ s^{-1}. When 550 nm excitation is used, the buildup of the $ZnTPP^+-PI^-$ population from S_1 is relatively slow ($\tau = 17$ ps), while the recombination rate to ^{3}*ZnTPP is comparable ($\tau = 18$ ps), so that the concentration of $ZnTPP^+-PI^-$ during the time course of the reaction is relatively low, as is indicated by the transient spectra and kinetics in Figures 1A and 2A, respectively. On the other hand, the much more rapid formation of $ZnTPP^+-PI^-$ following 420 nm excitation results in a large initial concentration of the radical ion pair that is revealed by the spectra and kinetics in Figures 1B and 2A, respectively. The formation of ^{3}*ZnTPP with $\tau = 18$ ps is reflected in the rise component necessary to fit the transient absorption data obtained at 480 nm, where ^{3}*ZnTPP absorbs strongly, Figure 2B.[40] The corresponding energy gap between $ZnTPP^+-PI^-$ and ^{3}*ZnTPP is much larger in toluene, Figure 9B, so that biexponential decay kinetics are not observed.

Comparing the charge separation rate constants from S_1 for ZnTPP−PI vs ZnTPP−β-PhPI in MTHF, the rate for PI at the *meso* position is 5.8 times faster than that for PI at the β position. On the other hand, the corresponding comparison of charge separation rates from S_2 show that the rate for ZnTPP−PI is 3.5 times *slower* than that for ZnTPP−β-PhPI. Comparing the charge recombination rates to ground state for $ZnTPP^+-PI^-$ vs $ZnTPP^+-\beta$-$PhPI^-$ in MTHF, the CR rate for $ZnTPP^+-PI^-$ is 2.6 times faster than that of $ZnTPP^+-\beta$-$PhPI^-$. The corresponding comparisons in toluene show similar trends albeit with smaller differences. The results strongly suggest that the a_{2u} orbital with significant electron density at the *meso* positions dominates the electronic coupling matrix elements for both charge separation from S_1 and charge recombination. These results are consistent with earlier observations concerning the role of the porphyrin a_{1u} and a_{2u} orbitals.[11,12,15] Yet, this effect is reversed for charge separation from the S_2 state. Configurational mixing within the S_2 state produces an electronic distribution that places more electron density on the β rather than the *meso* position.[15,16] This shift in electronic distribution results in faster rates of charge separation from the zinc porphyrin S_2 state for PI attached to the β position, which has not been observed previously.

Conclusions

Our transient absorption studies show that efficient electron transfer occurs from S_2 of ZnTPP to PI in these porphyrins despite the presence of the intervening phenyl between the zinc porphyrin macrocycle and the PI acceptor. This significantly increases the overall distance of the charge separation reaction relative to systems in which the PI is bound directly to the porphyrin macrocycle.[7] Our results also show that the relative rates of charge separation to an electron acceptor can be modified in an opposing fashion through attachment of the acceptor to either the *meso*- or β-pyrrole positions of the macrocycle, where the relative ordering of rates depends on whether the electron transfer proceeds from S_1 or S_2. This ordering correlates well with the larger calculated contribution of the metalloporphyrin a_{2u} orbital to S_1 and the a_{1u} orbital to S_2.[15] In addition, the decrease in the relative rate ratios observed in toluene relative to those in MTHF is most likely a consequence of solvent modulation of the a_{2u} and a_{1u} orbital energies.[16] This diversity of properties will allow us to design more complex donor−acceptor systems in which wavelength selective formation of S_1 or S_2 will produce different ion pair states with different spectroscopic observables. This type of behavior may prove useful in developing systems for information processing using ultrafast electron-transfer reactions within donor−acceptor molecules.

Acknowledgment. This work was supported by the National Science Foundation (Grant CHE-0102351) and the Office of Naval Research (Grant N00014-02-1-0381).

Supporting Information Available: Transient absorption spectra of ZnTPP in MTHF at 0.4 and 20 ps following a 420 nm laser pulse (Figure S1). This material is available free of charge via the Internet at http://pubs.acs.org.

References and Notes

(1) Aaviksoo, J. F. A.; Savikhin, S.; Stelmakh, G. F.; Tsvirko, M. P. *Chem. Phys. Lett.* **1984**, *111*, 275−278.

(2) Chosrowjan, H. T. S.; Okada, T.; Takagi, S.; Arai, T.; Tokumaru, K. *Chem. Phys. Lett.* **1995**, *242*, 644−649.
(3) Gurzadyan, G. G.; Tran-Thi, T. H.; Gustavsson, T. *J. Chem. Phys.* **1998**, *108*, 385−388.
(4) Vlcek, A. *Chemtracts* **2000**, *13*, 776−779.
(5) Gurzadyan, G. G.; Tran-Thi, T.; Gustavsson, T. In *New Trends in Atomic and Molecular Spectroscopy*; Gurzadyan, G. G., Karmenyan, A. V., Eds.; SPIE−The International Society of Optical Engineers: Bellingham, WA, 2000; Vol. 4060.
(6) Mataga, N.; Shibata, Y.; Chosrowjan, H.; Yoshida, N.; Osuka, A. *J. Phys. Chem. B* **2000**, *104*, 4001−4004.
(7) Mataga, N.; Chosrowjan, H.; Taniguchi, S.; Shibata, Y.; Yoshida, N.; Osuka, A.; Kikuzawa, T.; Okada, T. *J. Phys. Chem. A* **2002**, *106*, 12191−12201.
(8) LeGourrierec, D.; Andersson, M.; Davidsson, J.; Mukhtar, E.; Sun, L.; Hammarstrom, L. *J. Phys. Chem. A* **1999**, *103*, 557−559.
(9) Andersson, M.; Davidsson, J.; Hammarstrom, L.; Korppi-Tommola, J.; Peltola, T. *J. Phys. Chem. B* **1999**, *103*, 3258−3262.
(10) Mataga, N. C. H.; Shibata, Y.; Yoshida, N.; Osuka, A.; Kikuzawa, T.; Okada, T. *J. Am. Chem. Soc.* **2001**, *123*, 12422−12423.
(11) Weiss, C.; Kobayashi, H.; Gouterman, M. *J. Mol. Spectrosc.* **1965**, *16*, 415−450.
(12) Fajer, J.; Borg, D. C.; Forman, A.; Dolphin, D.; Felton, R. H. *J. Am. Chem. Soc.* **1970**, *92*, 3451−3459.
(13) Holten, D.; Bocian, D. F.; Lindsey, J. S. *Acc. Chem. Res.* **2002**, *35*, 57−69.
(14) Tsai, H.; Simpson, M. C. *Chem. Phys. Lett.* **2002**, *353*, 111−118.
(15) Petke, J. D.; Maggiora, G. M.; Shipman, L. L.; Christoffersen, R. E. *J. Mol. Spectrosc.* **1978**, *71*, 64−84.
(16) Davis, M. S.; Forman, A.; Fajer, J. *Proc. Natl. Acad. Sci. U.S.A.* **1979**, *76*, 4170−4174.
(17) Therien, M. J.; Dimagno, S. G. *PCT Int. Appl.* **1994**, 62 pp.
(18) Callot, H. J.; Schaeffer, E. *J. Chem. Res.* **1978**, *2*, 51.
(19) Yoshida, N.; Shimidzu, H.; Osuka, A. *Chem. Lett.* **1998**, *1*, 55−56.
(20) Callot, H. J. *Bull. Soc. Chim. Fr.* **1974**, *7−8*, 1492−1496.
(21) Lukas, A. S.; Miller, S. E.; Wasielewski, M. R. *J. Phys. Chem. B* **2000**, *104*, 931−940.
(22) Greenfield, S. R.; Wasielewski, M. R. *Opt. Lett.* **1995**, *20*, 1394−1396.
(23) Marquardt, D. W. *J. Soc. Ind. Appl. Math.* **1963**, *11*, 431−441.
(24) Gosztola, D.; Niemczyk, M. P.; Svec, W.; Lukas, A. S.; Wasielewski, M. R. *J. Phys. Chem. A* **2000**, *104*, 6545−6551.
(25) Greenfield, S. R.; Svec, W. A.; Gosztola, D.; Wasielewski, M. R. *J. Am. Chem. Soc.* **1996**, *118*, 6767−6777.
(26) Marcus, R. A. *J. Chem. Phys.* **1965**, *43*, 679.
(27) Wiederrecht, G. P.; Niemczyk, M. P.; Svec, W. A.; Wasielewski, M. R. *J. Am. Chem. Soc.* **1996**, *118*, 81−88.
(28) Yamada, K.; Imahori, H.; Yoshizawa, E.; Gosztola, D.; Wasielewski, M. R.; Sakata, Y. *Chem. Lett.* **1999**, *3*, 235−236.
(29) Yamazaki, T.; Yamazaki, I.; Osuka, A. *J. Phys. Chem. B* **1998**, *102*, 7858−7865.
(30) Osuka, A.; Marumo, S.; Maruyama, K.; Mataga, N.; Tanaka, Y.; Taniguchi, S.; Okada, T.; Yamazaki, I.; Yoshinobu, N. *Bull. Chem. Soc. Jpn.* **1995**, *68*, 262−276.
(31) Osuka, A.; Nakajima, S.; Maruyama, K.; Mataga, N.; Asahi, T. *Chem. Lett.* **1991**, *6*, 1003−1006.
(32) Imahori, H.; Yamada, K.; Hasegawa, M.; Taniguchi, S.; Okada, T.; Sakata, Y. *Angew. Chem., Int. Ed. Engl.* **1997**, *36*, 2626−2629.
(33) Harrison, R. J.; Pearce, B.; Beddard, G. S.; Cowan, J. A.; Sanders, J. K. M. *Chem. Phys.* **1987**, *116*, 429−448.
(34) Debreczeny, M. P.; Svec, W. A.; Wasielewski, M. R. *Science* **1996**, *274*, 584−587.
(35) Wasielewski, M. R.; Johnson, D. G.; Svec, W. A.; Kersey, K. M.; Minsek, D. W. *J. Am. Chem. Soc.* **1988**, *110*, 7219−7221.
(36) Wiederrecht, G. P.; Svec, W. A.; Wasielewski, M. R.; Galili, T.; Levanon, H. *J. Am. Chem. Soc.* **2000**, *122*, 9715−9722.
(37) Pekkarinen, L.; Linschitz, H. *J. Am. Chem. Soc.* **1960**, *82*, 2407−2411.
(38) Yu, H.-Z.; Baskin, S.; Zewail, A. H. *J. Phys. Chem. A* **2002**, *106*, 9845−9854.
(39) Jortner, J. *J. Chem. Phys.* **1976**, *64*, 4860−4867.
(40) Pekkarinen, L.; Linschitz, H. *J. Am. Chem. Soc.* **1960**, *82*, 2407−2411.